The Cold Spray Method

Subjects: Others

Contributor: Fabian Cezar Lupu , Corneliu Munteanu , Adrian Constantin Sachelarie , Vlad Nicolae Arsenoaia , Bogdan Istrate

The cold, thermal spraying technology “Cold Spray” is a method of processing particles in a solid state. Research conducted through cold spray technology has seen a significant improvement in material properties; when processing the particles in a solid state, they adhere to the surface instead of eroding it. Cold spraying has proven to be an effective technique for improving material properties, as confirmed by its integration into different fields and industries, becoming competitive by being the only method for depositing particles below their melting point.

cold spray microstructure mechanical properties

1. Introduction

The interest given to the improvement of the properties of materials through modern spraying methods, from which numerous pieces of research have been carried out, is reflected in the technological progress that has been made, presenting a continuous development of both the spraying installations and the powders used. At the same time, the desire to contribute to scientific progress through this technology development has exposed the potential of using surface spraying methods, such as cold spraying, on different types of materials that are subject to severe operating conditions, including the AISI 52100 steel used in the manufacture of bearings, ball screws, etc., as well as the various materials used in the military sector, where, for example, in the case of the manufacture of armor, most are made of homogeneous plates of laminated steel. These are strengthened by the heat treatments of quenching and tempering, which leads to obtaining a hardness of 28–35 HRC [1]. Concerns in this area are derived from mechanical performance deficiencies (and more) and opting for thermal spraying is an increasingly common alternative for redepositing and improving material characteristics. In an article, Champagne claims that this spraying technology (cold spraying) is revolutionary due to the fact that the improvement of the powders has led to the spraying of materials for which it is impossible to give heat treatment.

This technology has proven to be quite effective in the technological processes of repairing various components, as confirmed by the continuous development of both the spraying technology and the powders used in this process [2].

The cold spray approach enables low porosity coatings while retaining the feedstock powder’s phase composition. In contrast to thermally sprayed coatings, oxide formation and thermal stresses in the cold sprayed coatings are reduced or entirely eliminated since the working gas temperature during CS is always lower than the melting point of the sprayed material [3]. Thermal spraying is a cost-effective technique for creating thick coatings that may cover

any surface and can be created utilizing a greater variety of feedstock materials. Complete or partial melting of the feedstock materials is required for thermal spray technologies, like flame spraying, high-velocity oxy-fuel spraying, and plasma spraying. This can lead to high residual stress in the coatings and material oxidation when the spraying process is carried out in an ambient atmosphere [4][5]. Through this method, the feedstock powder microstructures and characteristics are preserved, preventing oxide formation and other unfavorable structural changes, and improving the longevity of the coatings. Due to the plastic deformation brought on during deposition, cold-sprayed materials have harder surfaces than their equivalent powders and bulk alloys [6].

2. Studies Using the Cold Spray Method

When using the cold spray technique, thanks to its many benefits, a variety of industrial items, including turbine blades, pistons, cylinders, bearing components, and shafts, may be produced and repaired. Different coatings can contribute to the features, including hardness, wear and corrosion resistance, and heat conductivity [7].

Trials show that the cold spraying of W is rather ambitious due to the metal's hardness and brittleness at very high temperatures. In contrast, cold spraying can create thick and very dense tantalum (Ta) coatings, which are already used in the space, chemical, and nuclear industries, as well as in medical applications. Metallographic cross-sections of the coatings created by the separate feeding of coarse W and Ta, where 2 mm-thick coatings were produced from the powder, are shown in the microscopic photographs in **Figure 1**. All of the coatings exhibit little porosity and a growing W volume fraction with an increasing W powder percent, as can be seen from the images [8][9].

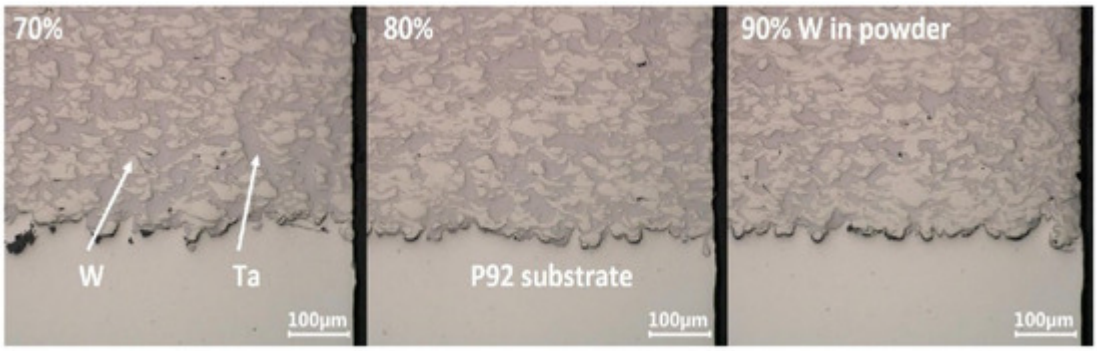

Figure 1. Cold spray coatings with varying amounts of tungsten and tantalum, as seen in metallographic cross-sections [8].

The feedstock powder and the high gas consumption rate are the two main cost factors in cold spray technology. Helium has the advantages of efficiency and a high-quality microstructure, but it is also costly. However, nitrogen, the most often researched cold spray propellant gas, is quite affordable [10].

2.1. Types of Materials Used for Cold Spray

Of the many types of materials available, for example, ARMOX ballistic plates are produced by metallurgy based on iron ore and through blast furnaces, deoxidized steel in an LD converter and with vacuum treatment results in very clean steel. Through high-tech rolling mills, a fine-grained microstructure is obtained and finally, to obtain the desired hardness/strength properties, the steel is subjected to various specific heat treatments [11][12].

ARMOX plates can be found in a range of hardnesses from homogeneous rolled steel, with a hardness of 280 BHN, to UHH steel, with a hardness of more than 640 BHN, and these are mainly used together with materials such as steel, aluminum, composite materials, etc. [11]. The chemical compositions are presented in **Table 1**, and the mechanical properties are presented in **Table 2** for several types of plates, namely Armox 500 T, Armox 600 T, and Armox Advance [13].

Table 1. Chemical composition of ARMOX plate [11].

Name	C Max(%)	Si Max (%)	Mn Max (%)	P Max (%)	S Max (%)	Cr Max (%)	Ni Max (%)	Mo Max (%)	B Max (%)
Armox 500 T	0.32	0.40	1.20	0.010	0.003	1.0	1.80	0.70	0.005
Armox 600 T	0.47	0.70	1.0	0.010	0.003	1.5	3.0	0.70	0.005
Armox advance	0.47	0.70	1.0	0.010	0.003	1.5	3.0	0.7	0.005

Table 2. Mechanical properties of ARMOX plate [12].

Name	Hardness (BHN)	0.2% Yield Strength (N/mm^2)	Tensile Strength (N/mm^2)	Elongation (%)
Armox 500 T	480–540	min 1250	1450–1750	Min 8
Armox 600 T	570–640	1500	2000	7
Armox advance	HRC58-63	1600	2250	9

Poplawski et al. investigated the fracture properties of Armox 500 T steel with respect to perforation problems through an experimental, numerical procedure to develop the fracture surface in triaxiality and Lode parameter space. The tests performed (including FEM tests, in addition to the practical ones) on several types of samples using three types of punches (pointed, flat, and hemispherical), perforating 1 mm plates, show a sensitivity regarding the Lode parameter, such that the fracture properties depend on this parameter. The greatest force required for perforation was exerted on the hemispherical punch, then the flat one, followed by the pointed one. By means of a Kedzierski model, the highest force obtained was intensified to be between the results of Skoglund's and Iqbal's fracture models. The perforated plates are shown in **Figure 2** [14].

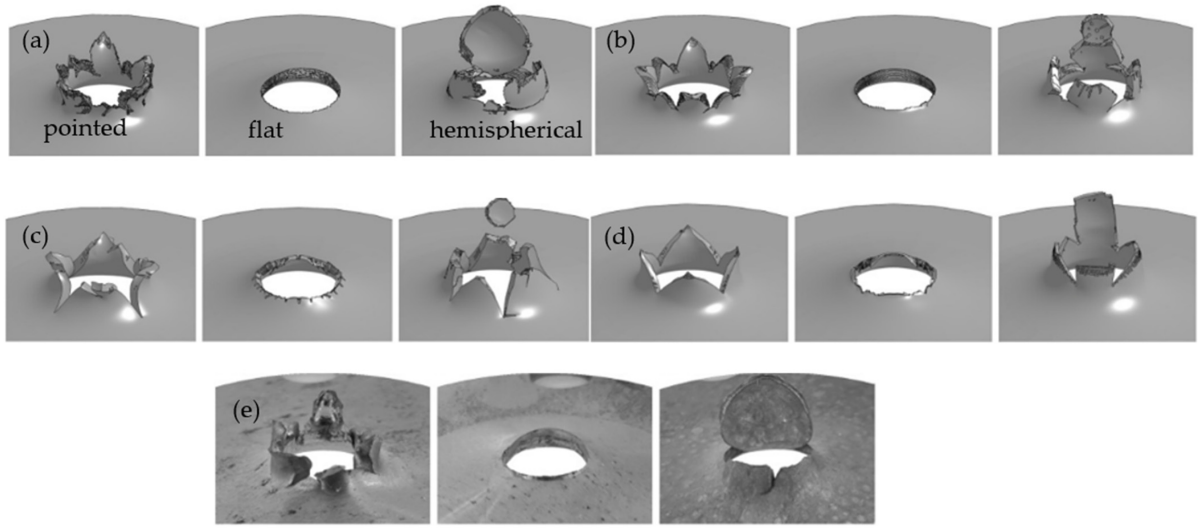

Figure 2. (**a**) FEM present study; (**b**) FEM Kedzierski; (**c**) FEM iqbal; (**d**) FEM Skoglund; (**e**) Experiment [14].

In **Figure 3** [14], the first trial of the experiment is represented with a solid gray line, a dotted line for the second trial of the experiment, as well as a double-dotted line for the third trial of the experiment, with a solid yellow line for the FEM analysis of the present study, a solid blue line for the FEM analysis of the Skoglund model, a solid green line for the FEM analysis of the Iqbal model, and a solid red line for the FEM analysis of the Kedzierski model.

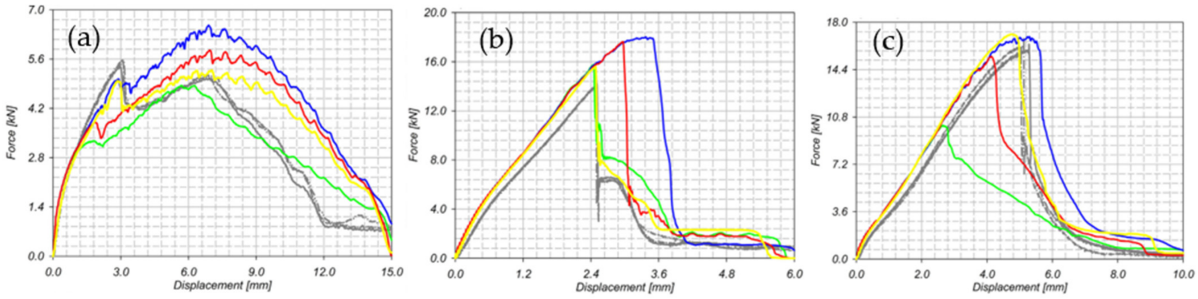

Figure 3. Measured plate punching forces: (**a**) sharp punch, (**b**) flat punch, and (**c**) hemispherical punch [14].

2.2. Cold Spray Method

Like many materials with high properties, 52100 steel, for example, is distinguished by mechanical properties with respect to elastic stiffness. It has a modulus of elasticity that manages to present high values, namely 210 GPa, leading to the formation of a resistant material while, at the same time, responding well when subjected to processing processes. It also exhibits important properties regarding compressive strength; for example, despite being almost twice as hard as most aluminum alloys, it has a bulk modulus value of 160 GPa. Both the physical and mechanical properties of this type of steel give it properties that make it an excellent material for making parts that must withstand extreme pressures, such as ball screws, aviation bearings, and so on [15][16].

For a better understanding, Kiranbabu et al. approached the mechanism of carbide decomposition in steel 52100 (100Cr6), a mechanism that is crucial for obtaining corrosion-resistant steels that are encountered in industrial

applications. The decomposition of cementite is investigated through a modified thermal treatment in order to generate a soft, annealed microstructure in which spherical cementite and lamellar cementite precipitate. In order to investigate the effects of the composition, morphology, and size, as well as the microstructure of the matrix in order to decompose the cementite, the microstructure was subjected to a severe plastic deformation induced by HPT (p = 7.56 GPa, Ymax~50). After the investigations, it was concluded that adding Cr and Mg leads to an increase in the stability of cementite. Regarding the wear of the spherical cementite precipitates, no wear was observed, with the pearlitic matrix presenting a hardness of 4.7 GPa (in view of the wear behavior, the decisive role is the hardness of the matrix around the precipitates). In **Figure 4**, the Y~50 lamella is shown, whereas **Figure 4**a represents the deformed spherical cementite, and **Figure 4**b shows the precipitate of the deformed spherical cementite from **Figure 4**a. A precipitate smaller than (~100 nm) does not indicate any internal deformation [17][18].

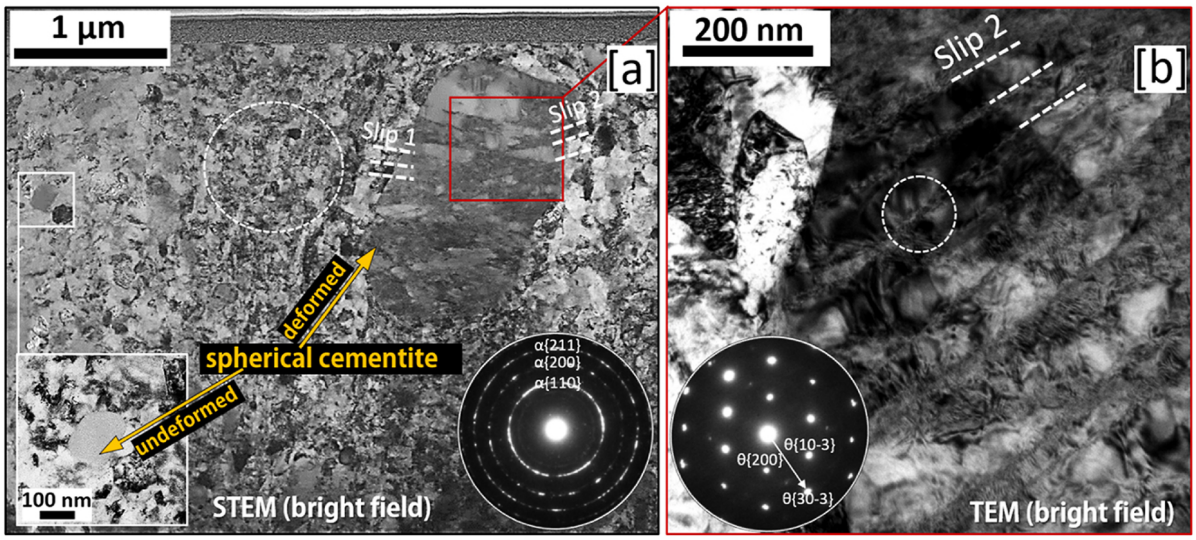

Figure 4. TEM image with diffraction analysis of sample Y~50. (**a**) deformed spherical cementite; (**b**) precipitate of deformed spherical cementite [17].

In research conducted by Rahbar et al., a 52100-steel substrate using WC-12%Co that was thermally sprayed before friction stir processing (FSP) was carried out on this layer. Before and after FSP, the wear resistance and hardness were tested. FSP combines the sprayed layer with the substrate and lowers porosity and improves hardness and wear performances, according to optical and SEM analysis. Three various structures of the as-sprayed layer are shown in **Figure 5**a; the WC-12%Co layer is the top porous layer; for improved adhesion, the intermediate layer is a Ni-Al composite, and the bottom layer is the base metal. According to **Figure 5**b, the refined zone, which contains martensite and WC particles, extends to about 1.2 mm below the surface of the sprayed layer following FSP. The WC is dispersed in a martensitic matrix in this image. When comparing the FSPed structure to the as-sprayed structure, neither the layer boundaries nor the porosity are clearly defined. Since a totally dense microstructure was created by the thermo-mechanical deformation, FSP has solved two drawbacks of sprayed layer: porosity and poor adhesion. The WC particle size is shown in **Figure 5**c,d, respectively, before and after the FSP. It is obvious that the FSP treatment may reduce the original WC particles to submicron size, and this will affect the hardness and wear performance. During FSP, the smaller WC particles may also experience plastic flow

in a Co binder at high temperatures, which would promote a completely thick microstructure and improve WC particle spreading. This would provide a high microhardness [19].

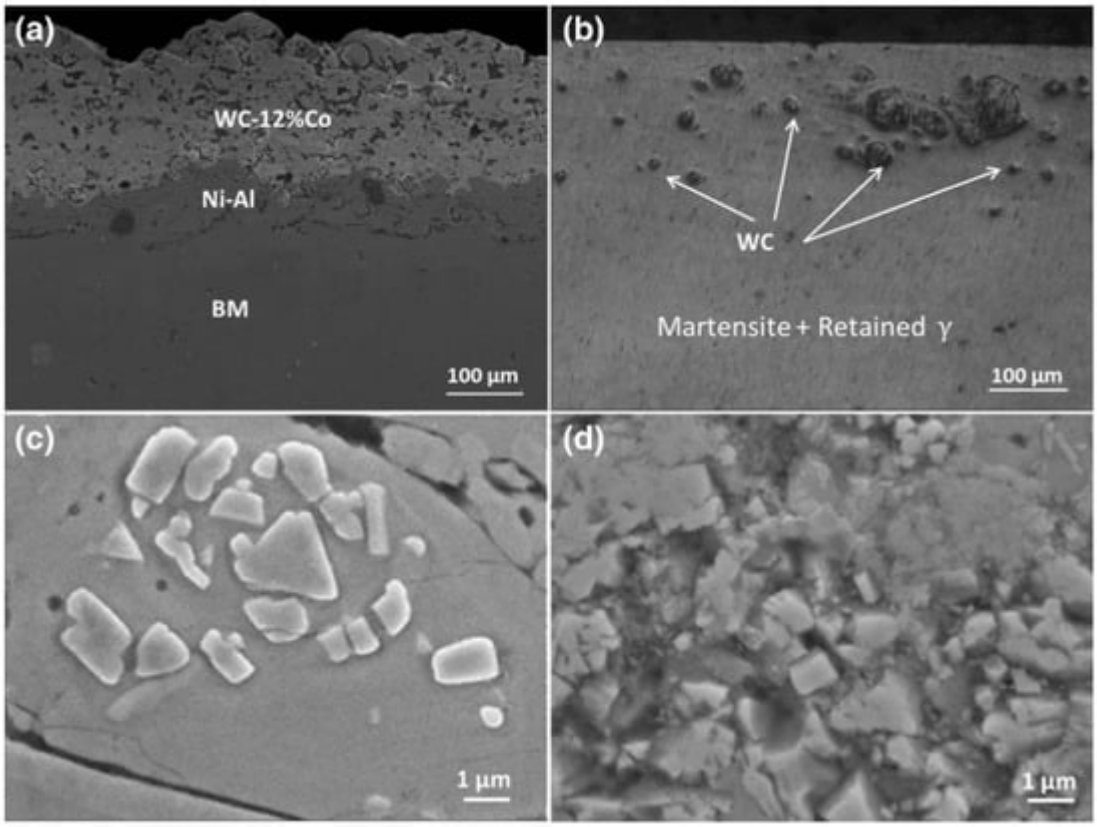

Figure 5. The WC particle size (**c**) before and (**d**) after FSP, as well as the structure of the sprayed layer (**a**) before and (**b**) after FSP [19].

In research conducted by Agiwal et al., in which they repaired the cracks in a 304 L austenitic stainless steel in the field, two methods were investigated: cold spray deposition (CSD) and friction surfacing (FS). Both of these solid-state, low-heat-input methods avoid the negative impacts of solidification, such as compositionally segregated microstructures and shrinkage stresses. Cross-sectional pictures of the coating/substrate contacts fixed by the two procedures are shown in **Figure 6**. In the steady-state zone, friction surfacing with the consumable rod generated coatings that were 325 µm thick and 2.3 mm broad. The absence of porosity in the coatings and the smooth interface between the coating and substrate point to a strong connection. **Figure 6**c demonstrates how the FS procedure may patch a fictitious crack. At a depth of 75 µm below the coating/substrate contact, the fracture point was seen to bow. High compressive residual stresses at the surface caused by friction surfacing are thought to have contributed to the substrate's plastic deformation and fracture bending and closing. A high-density cold spray coating (porosity level of less than 0.3%) is seen covering the through-crack in **Figure 6**b. The coating had a ~620 µm thickness. As it got closer to the coating/substrate contact, the crack's breadth shrank. At a distance of approximately ~90 µm above the coating/substrate contact, the hairline fracture ultimately vanished. As seen in **Figure 6**d, some severely damaged powder particles were discovered inside the through-crack. Two potential processes for repairing cracks include compressive stress from the CSD process and the deformation of the substrate at the fracture opening, followed by the application of a stainless-steel coating. For example, the

substrate may become smaller as a result of the lateral displacement it experiences as a result of the powder particles striking it at the crack opening. Due to peening action, complete coverage of the coating may be accomplished during the succeeding particle impact once the crack-opening size is less than the powder particle size (<44 µm). Phase preservation and the lack of deformation-induced martensite distinguish the cold spray coatings from the friction-surfaced coatings [20][21].

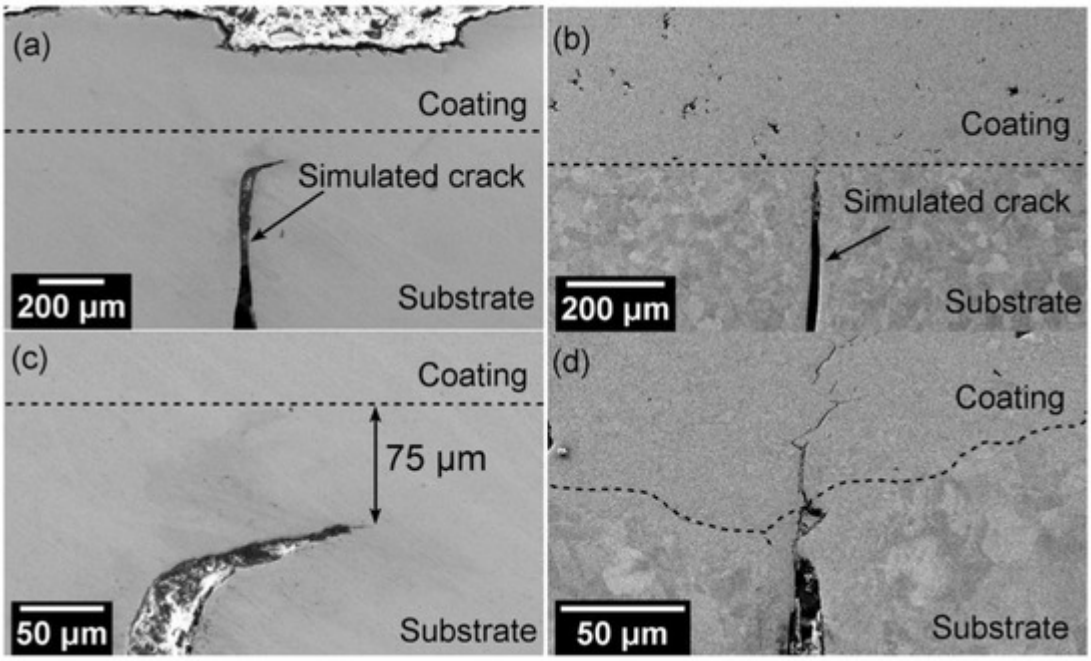

Figure 6. SEM cross-sectional pictures of areas that were restored using cold spray deposition (**b**,**d**) and friction surfacing (**a**,**c**) [20].

Wenpeng et al. carried out a study due to the requirements of the spray gun to be able to facilitate the control of the spray for a long time; these requirements were found due to the studies that attest to the fact that the spray injector (the component that is part of the gun assembly) leads to a disturbance in the flow fields and the parameters of the particle impact. After the tests were carried out, it was concluded that the size of the particles, the diameter of the spray hole of the injector, and the pressure discrepancy between the gas supplying the powder and the main working gas led to a significant influence on the distribution of the particles both near the neck of the spray nozzle and in front of the substrate. **Figure 7** illustrates how the particle deposition range on the substrate grows as the injector's inner diameter decreases. In addition, as the injector's inner diameter grows, so does the gradient of the particle departure from the nozzle axis upstream of the nozzle. As a result, the powder injector with a smaller inner diameter can, in the CSAM process, not only increase the production accuracy of parts but also, to a certain extent, lessen the likelihood of nozzle blockage or sticking upstream of the nozzle [22][23].

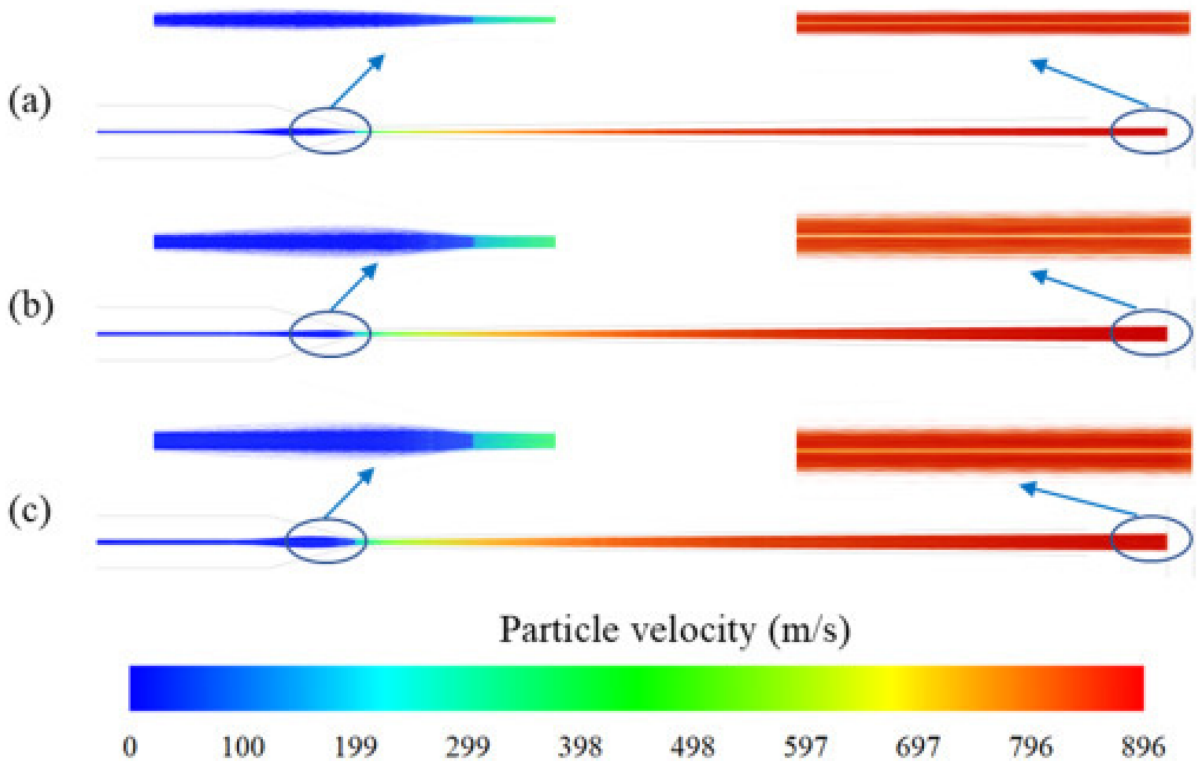

Figure 7. Particle tracks at different inner diameters of the powder injector are colored according to the particle velocity: (**a**) 0.5 mm; (**b**) 1 mm, and (**c**) 1.5 mm. The sizes of the particles range from 5 to 60 m [22].

Through these tests, it was highlighted that the improvement of the impact speed of the particles, as well as a reduction in the risk of clogging the nozzle with a concentration of particles near it, are optimized by reducing the internal diameter of the powder injector and by using a pressure that is smaller than the differentials; at the same time, the use of particles with diameters between 20–40 µm lead to an improvement in precision [22].

An important aspect of this surface spraying technology is that it expands the range of applications in terms of thermal spraying, something that is applicable in industries such as automotive, aerospace, medical, and petrochemical, helping to both produce and restore various components, such as defects processing, casting, and even the possibility of remaking the mold [24].

References

1. Cristea, S. Contributii la Studiul Comportarii Unor Materiale de Blindaj la Impactul cu Proiectilul. Ph.D. Thesis, Lucian Blaga University, Sibiu, Romania, 2008.
2. Phillips Federal News. Available online: https://phillipscorp.com/federal/2020/06/24/vrc-army-phillips-federal/ (accessed on 6 September 2022).
3. Shikalov, V.S.; Vidyuk, T.M.; Filippov, A.A.; Kuchumova, I.D. Microstructure, mechanical and tribological properties of cold sprayed Cu-W coatings. Int. J. Refract. Met. Hard Mater. 2022, 106,

105866.

4. Wei, F.J.; Chou, B.Y.; Fung, K.Z.; Tsai, S.Y. Thermomechanical properties of cold-sprayed copper coatings from differently fabricated powders. Surf. Coat. Technol. 2022, 434, 128128.
5. Ranjan, R.; Das, A.K. A review on surface protective coating using cold spray cladding technique. Mater. Today Proc. 2022, 56, 768–773.
6. Poza, P.; Maneiro, M.A.G. Cold-sprayed coatings: Microstructure, mechanical properties and wear behaviour. Prog. Mater. Sci. 2022, 123, 100839.
7. Champagne, V.K. The Cold Spray Materials Deposition Process: Fundamentals and Applications; Woodhead: Cambridge, UK, 2007; p. 376.
8. Neu, R.; Maier, H.; Boswirth, B.; Elgeti, S.; Greuner, H.; Hunger, K.; Kondas, J.; Muller, A. Investigations on cold spray tungsten/tantalum coatings for plasma facing applications. Nucl. Mater. Energy 2022, 34, 101343.
9. Jan, C.; Monika, V.; Frantisek, L.; Martin, K.; Jan, K.; Reeti, R.S. Cold Sprayed Tungsten Armor for Tokamak First Wall. Coatings 2019, 9, 836.
10. Yeom, H.; Sridharan, K. Cold spray technology in nuclear energy applications: A review of recent advances. Ann. Nucl. Energy 2021, 150, 107835.
11. SSAB. Available online: https://www.ssab.com/en (accessed on 7 September 2022).
12. Dwight, D.S.; William, A.G.; Mattew, S.B.; Stockman, R.K. Balistic Testing of SSAB Ultra-High-Hardness Stell for Armour Applications; Army Research Laboratory: Adelphi, MD, USA, 2008.
13. Olimpicsteel. Available online: https://www.olysteel.com/products/alloy/mil-dtl-46100-mil-a-46100-armor-steel (accessed on 7 September 2022).
14. Poplawski, A.; Kedzierski, P.; Mork, A. Identification of Armox 500T steel failure properties in the modeling of perforation problems. Mater. Des. 2020, 190, 108536.
15. Alloy Steel 52100. Available online: https://continentalsteel.com/carbon-steel/grades/alloy-52100/ (accessed on 21 September 2022).
16. Panda, A.; Sahoo, A.K.; Kumar, R.; Das, R.K. A review on machinability aspects for AISI 52100 bearing steel. Mater. Today Proc. 2020, 23, 617–621.
17. Kiranbabu, S.; Tung, P.Y.; Sreekala, L.; Prithiv, T.S.; Hickel, T.; Pippan, R.; Morsdorf, L.; Herbig, M. Cementite decomposition in 100Cr6 bearing steel during high-pressure torsion: Influence of precipitate composition, size, morphology and matrix hardness. Mater. Sci. Eng. A 2022, 833, 142372.
18. Qin, Y.; Mayweg, D.; Tung, P.Y.; Pippan, R.H. Mechanism of cementite decomposition in 100Cr6 bearing steels during high pressure torsion. Acta Mater. 2020, 201, 79–93.

19. Rahbar-Kelishami, A.; Abdollah-Zadeh, A.; Hadavi, M.M.; Benerji, A.; Alpas, A.; Gerlich, A.P. Effects of friction stir processing on wear properties of WC-12%Co sprayed on 52100 steel. Mater. Des. 2015, 86, 98–104.
20. Agiwal, H.; Yeom, H.; Pocquette, N.; Sridharan, K.; Pfefferkorn, F.E. Friction surfacing and cold spray deposition for surface crack repair in austenitic stainless steels. Mater. Today Comun. 2022, 33, 104692.
21. Yeom, H.; Dabney, T.; Pocquette, N.; Ross, K.; Pfefferkorn, F.E.; Sridharan, K. Cold spray deposition of 304L stainless steel to mitigate chloride-induced stress corrosion cracking in canisters for used nuclear fuel storage. J. Nucl. Mater. 2020, 538, 152254.
22. Wan, W.; Li, W.; Wu, D.; Qi, Z.; Zhang, Z. New insights into the effects of powder injector inner diameter and overhang length on particle accelerating behavior in cold spray additive manufacturing by numerical simulation. Surf. Coat. Technol. 2022, 444, 128670.
23. Lupoi, R.; Neill, W. Powder stream characteristics in cold spray nozzles. Surf. Coat. Technol. 2011, 206, 1069–1076.
24. Singh, H.; Sidhu, T.S.; Kalsi, S.B.S. Cold spray technology: Future of coating deposition processes. Frat. Integrità Strutt. 2012, 22, 69–84.